

Satellite Tracking System using Amateur Telescope and Star Camera for Portable Optical Ground Station

Hyosang Yoon, Kathleen Riesing, and Kerri Cahoy
 Department of Aeronautics and Astronautics, Massachusetts Institute of Technology
 77 Massachusetts Avenue, Cambridge, MA 02139
 hyosang@mit.edu

ABSTRACT

As CubeSat capabilities continue to improve, many missions need high-speed communication to downlink data. Data rates using radio frequency (RF) communications are constrained by antenna size and power. Laser communications (lasercom) systems can use a much narrower beam width for a given aperture size due to having shorter wavelengths. Higher data rates can be achieved with optical communication than with RF assuming the same power level and similar efficiencies, but the primary challenge of lasercom systems is the precise pointing required for link closure.

Optical communication requires higher pointing accuracy, not only for the transmitter but also for the receiver, because of the directionality of the laser beam. This means that an optical ground station must be able to track a satellite with high accuracy. For an optical ground station such as the Optical Communications Telescope Laboratory (OCTL) from the Jet Propulsion Laboratory (JPL) or the Optical Ground Station (OGS) of the European Space Agency (ESA), the telescope is part of a fixed facility, and its pointing can be precisely calibrated using stars over a long period of time. However, these meter-class optical ground stations have costs and logistical complexities similar to those of the large aperture RF ground stations currently used for CubeSats requiring high data rates.

To address this challenge, the MIT STAR Lab is developing a portable ground station with an amateur telescope for the Nanosatellite Optical Downlink Experiment (NODE) project. State of the art amateur telescopes provide good control capability with gimbals, but the user must align the gimbals with respect to an inertial, Earth-fixed frame. Even for an experienced amateur astronomer, this is a non-trivial problem, and it can take hours to get the fine alignment within a few arcminutes accuracy.

We propose a novel approach to track a satellite with an amateur telescope. To resolve the alignment problem, we use a wide field of view star camera to determine its orientation with respect to an inertial frame. Star sensors are accurate to the arcsecond level, and they have the advantage of providing orientation with a single measurement. Using multiple star sensor measurements at different gimbal angles, it is possible to calculate the alignment of the gimbals in the Earth-fixed frame and the alignment of the star sensor in the gimbal frame. Once the alignment is obtained, satellite tracking can be achieved easily with a known orbit and precise Earth rotation model such as the International Earth Rotation and Reference System Service (IERS). We present the alignment calibration method and the preliminary tracking results using a Celestron CPC 1100 XLT to validate our approach.

INTRODUCTION

Laser communications (lasercom) is growing in popularity due to the important advantages it offers over radio frequency (RF) communications. These advantages include high bandwidth, small size, low required power, secure transmission in a narrow beam, and a minimal regulatory environment.

While lasercom has been demonstrated in high profile missions such as the Lunar Laser Communications Demonstration [1] and Laser Communication Terminal (LCT) to be used in the planned European Data Relay System [2], these terminals are intended for spacecraft

weighing hundreds of kilograms or more. Recent efforts have examined the use of lasercom on nanosatellites. Several systems have been proposed [3,4], including the Optical Communication and Sensor Demonstration (OCSD) from the Aerospace Corporation which aims to demonstrate a threshold 5 Mbps optical link from a 1.5-U CubeSat in low earth orbit (LEO) with a stretch goal of 500 Mbps [5]. As the increase in nanosatellites on orbit places pressure on RF spectrum allocation, lasercom is becoming an increasingly attractive option for nanosatellites.

Existing ground stations are typically in remote locations that share desirable characteristics with

astronomical observatories. Ground stations such as JPL's Optical Communications Telescope Laboratory (OCTL) on Table Mountain southern California and ESA's Optical Ground Station (OGS) concurrent with the Teide Observatory on Tenerife have been critical in lasercom demonstration missions to date [6,7].

As lasercom becomes a possibility for nanosatellites, there is a need for optical ground stations that share the characteristics of many nanosatellite programs: inexpensive, flexible, drawing from commercial-off-the-shelf (COTS) technology, and easily deployed with the opportunity for a rapid iteration cycle. Prior work in this area is limited. The German Aerospace Center (Deutsches Zentrum für Luft- und Raumfahrt; DLR) as developed the Transportable Optical Ground Station (TOGS) with a 60 cm aperture and a mass of

approximately 500 kg [8]. This system can be transported and unloaded from a van and has successfully demonstrated 1.25 Gbps communication with an aerial platform [9].

We consider the use of a commercial amateur telescope as a portable optical ground station. In this paper, we describe the development of software to autonomously calibrate the telescope with a star tracker and to drive the telescope to track a satellite in LEO. Results from tracking the International Space Station (ISS) with this approach are presented.

TRACKING SYSTEM DESIGN

The NODE ground station (GS) consists of two parts: the tracking system and the receiver. Figure 1 shows the block diagram of the GS.

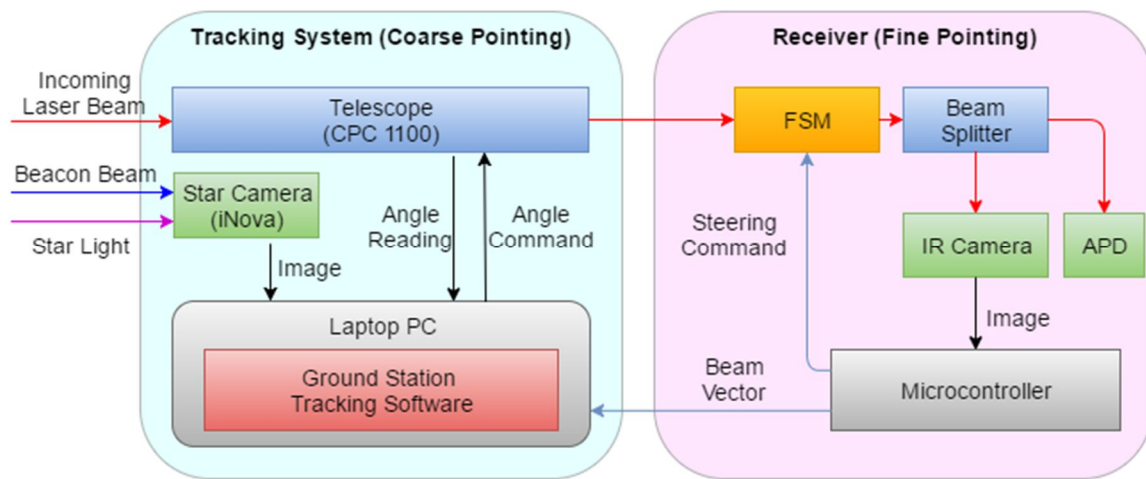


Figure 1: Block diagram of portable optical ground station.

The ground station fine pointing system is not discussed in detail here and will be discussed in future work. It consists of a fast steering mirror (FSM), infrared (IR) camera for fine tracking, and an avalanche photodiode (APD) receiver. Once the laser signal is captured by the IR camera, the pointing vector to the satellite can be calculated very accurately, to better than one arcsec. This measurement allows the ground station to accurately point the beam using the telescope mount and the FSM. The goal for the tracking (coarse pointing) system, is to track the satellite well enough that the IR tracking camera can capture the laser signal and start the fine pointing.

The tracking system consists of the star camera, the telescope mount, and the ground station tracking software running on a laptop computer. The star camera is used for initial alignment calibration and

feedback control for satellite tracking. An astronomy camera, iNova PLB-Mx2, is used as the star camera with 35 mm focal length. The field of view (FOV) of the camera is 7.8 deg x 5.9 deg. This is wide enough to capture more than 7 stars which are brighter than 6.5 Mv in a single image. The telescope mount is the actuator of the tracking system. It is a COTS product that comes with the amateur telescope CPC 1100 from Celestron. The ground station tracking software is developed in-house at MIT STAR Lab. It uses the Simplified General Perturbations 4 (SGP4) orbit propagator [10] and an Earth model from the International Earth Rotation and Reference Systems Service (IERS) [11].

The first step of tracking is to obtain the alignment of the telescope with respect to the Earth-centered-Earth-fixed (ECEF) frame. This system is portable, which means its alignment must be calculated every

time the setup is moved. The CPC 1100 provides several embedded methods to calculate its alignment with respect to inertial frame using stars. Amateur astronomers use this built-in telescope alignment capability. However, this is not suitable for our system because the alignment accuracy is not reliably quantified and it highly depends on the user ability. Therefore, we use a star camera mounted on the telescope, which is essentially the same as a star tracker used for attitude determination in spacecraft. Figure 2 shows the telescope and the star camera.



Figure 2: Telescope and star camera.

By matching the pattern of stars captured by the star camera, we can calculate the orientation of the star camera frame with respect to an inertial frame such as J2000 at the image capture time. By taking multiple images over the sky, it is possible to calculate the alignment between the telescope frame and ECEF frame as well as the alignment between telescope and the star camera. The detailed algorithms are described in the following section.

Another issue for the initial alignment is obtaining the alignment between star camera and the actual line-of-sight (LOS) of the telescope. The telescope mount initializes its azimuth (Azi) and Altitude (Alt) angle as zero every time it is turned on, so the actual LOS is unknown to the telescope frame. Therefore, we need to calculate the LOS of the telescope frame every time the ground station is set up. To obtain the LOS, we use another astronomy camera, the Orion StarShoot USB Eyepiece II, to capture an image through the telescope. The star camera to telescope LOS could be calculated autonomously if images of star patterns could be taken with the eyepiece camera, but the FOV is too narrow for this to be possible. The focal length of the CPC 1100 is 2.8 m and the detector size of the eyepiece camera is 3.8 mm x 2.9 mm, so the FOV is 0.078 deg x 0.059 deg or 282 arcsec x 212 arcsec. It is hard to capture a star within this narrow field of view with unknown mount

angles. Therefore, we manually point the telescope at a distant, fixed light source on the ground with the eyepiece camera, take a picture using the star camera, and calculate the LOS vector in the camera frame. We could use a bright star rather than a ground object, but it is difficult to keep the star at the center of the narrow FOV due to sidereal motion. In our setup, we use a red beacon light on the top of a tall building in Boston across Charles River from an MIT building in Cambridge.

ALGORITHMS FOR ALIGNMENT

In this section, we describe the main algorithms used in the tracking system to calculate the alignment of the telescope.

Star Identification Algorithm

The stars must be identified in each frame of from the star camera. Star identification has been extensively researched for decades and a large number of algorithms have been proposed with different advantages. In this study, we implement a correlation-based star pattern matching algorithm proposed by Yoon et al. [12,13] The correlation algorithm is disadvantageous in terms of processing time since it calculates an exponential function for the matching-scores. However, it provides additional robustness with respect to the star center position error. While computation time is a concern for spacecraft with limited resources, it is suitable for our system which has a laptop with a 2.7 GHz CPU as a processing unit, and the additional robustness is important given that we have an uncalibrated star camera with a COTS lens. The identification algorithm matches the star pattern to a star catalog such as SKY 2000, and gives the corresponding star vectors in the J2000 frame. Since the star vectors are determined in the camera frame, we can simply calculate the attitude quaternion of the camera frame with respect to J2000 frame using the QUEST algorithm [14], which is also commonly used for spacecraft attitude determination from vector measurements. More details about the star identification algorithms and QUEST can be found in Ref. 12, 13, and 14.

Coarse Alignment Calibration

The alignment calibration is divided into two levels: coarse calibration and fine calibration. In coarse alignment calibration, we calculate the alignment quaternions without any prior information. The result is used as an initial value for the fine alignment calibration described in the next section.

Before describing the algorithms, the coordinate systems must be defined. There are three relevant frames: the gimbals frame, the star camera frame, and the telescope frame. The Y-axis of the gimbals frame is defined as the rotation axis of the Azi motor when the telescope is initialized. Likewise, the X-axis is defined as the rotation axis of the Alt motor when initialized. These correspond to zero Azi/Alt angles. The Z-axis of the gimbals frame is defined by the cross product of the X-axis and Y-axis. The telescope frame is initially aligned with the gimbals frame, but it is fixed to the telescope through Azi/Alt rotation. The Z-axis of the camera frame is defined by the LOS of the star camera and the X and Y axes are the star camera's lateral and vertical directions. Figure 3 illustrates the three frames.

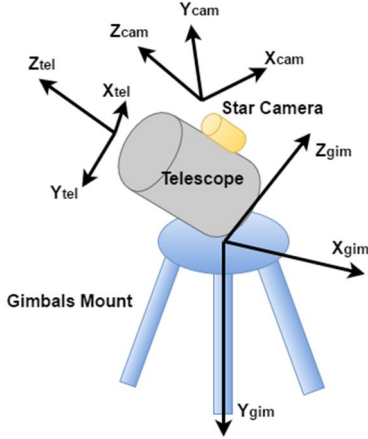


Figure 3: Definition of the gimbals frame, the star camera frame, and the telescope frame.

By the definition, the direction cosine matrix (DCM) from the gimbals frame to the telescope frame is given by

$${}^{tel}T_{gim} = \begin{bmatrix} 1 & 0 & 0 \\ 0 & ct & st \\ 0 & -st & ct \end{bmatrix} \begin{bmatrix} cz & 0 & -sz \\ 0 & 1 & 0 \\ sz & 0 & cz \end{bmatrix} \quad (1)$$

where cz and sz are the cosine and sine of Azi angle and ct and st are the cosine and sine of Alt angle, respectively. Note that the Z-axis of the telescope frame is not the same as the LOS of the telescope.

The sensor measurement is the attitude quaternion of the star camera, which corresponds to a DCM from J2000 frame to the star camera frame. The i -th star camera measurement can be written as

$$\bar{q}_{m,i} = \bar{q}_{n,i} \otimes {}^{cam}\bar{q}_{tel} \otimes {}^{tel}\bar{q}_{gim,i} \otimes {}^{gim}\bar{q}_{ecf} \otimes {}^{ecf}\bar{q}_{j2k,i} \quad (2)$$

where \otimes is the quaternion product operator as

$${}^c\bar{q}_A = {}^c\bar{q}_B \otimes {}^B\bar{q}_A \quad (3)$$

and $\bar{q}_{n,i}$ is a noise quaternion that models star camera measurement noise given as

$$\bar{q}_{n,i} \approx \begin{bmatrix} \vec{q}_{n,i} \\ 1 \end{bmatrix}, \quad E[\bar{q}_{n,i}] = 0, \quad E[\bar{q}_{n,i}\bar{q}_{n,i}^T] = \text{diag}(r_1, r_2, r_3) \quad (4)$$

In (2), ${}^{tel}\bar{q}_{gim,i}$ is calculated by (1) with the gimbals angle reading and ${}^{ecf}\bar{q}_{j2k,i}$ is calculated by the IERS model for the measurement time. Finally, ${}^{cam}\bar{q}_{tel}$ and ${}^{gim}\bar{q}_{ecf}$ are the two constant, unknown values that must be estimated from a set of measurements, $\bar{q}_{m,i}$. For convenience, define the measurement in ECEF frame as

$${}^{ecf}\bar{q}_{m,i} \triangleq \bar{q}_{m,i} \otimes {}^{ecf}\bar{q}_{j2k,i}^{-1} \quad (5)$$

To calculate ${}^{cam}\bar{q}_{tel}$, let us assume zero measurement noise and consider the difference quaternion between i -th and j -th measurements as the following:

$$\begin{aligned} & {}^{ecf}\bar{q}_{m,i} \otimes {}^{ecf}\bar{q}_{m,j}^{-1} \\ &= {}^{cam}\bar{q}_{tel} \otimes {}^{tel}\bar{q}_{gim,i} \otimes {}^{gim}\bar{q}_{ecf} \otimes ({}^{cam}\bar{q}_{tel} \otimes {}^{tel}\bar{q}_{gim,j} \otimes {}^{gim}\bar{q}_{ecf})^{-1} \\ &= {}^{cam}\bar{q}_{tel} \otimes {}^{tel}\bar{q}_{gim,i-j} \otimes {}^{cam}\bar{q}_{tel}^{-1} \\ &= \begin{bmatrix} A({}^{cam}\bar{q}_{tel}) & 0 \\ 0 & 1 \end{bmatrix} {}^{tel}\bar{q}_{gim,i-j} \end{aligned} \quad (6)$$

where

$${}^{tel}\bar{q}_{gim,i-j} = {}^{tel}\bar{q}_{gim,i} \otimes {}^{tel}\bar{q}_{gim,j}^{-1} \quad (7)$$

Since we have ${}^{ecf}\bar{q}_{m,i}$, ${}^{ecf}\bar{q}_{m,j}$, ${}^{tel}\bar{q}_{gim,i}$, and ${}^{tel}\bar{q}_{gim,j}$, we can calculate ${}^{cam}\bar{q}_{tel}$ using an attitude determination algorithm from vector measurement such as QUEST with 3 or more measurements. Likewise, we can calculate ${}^{gim}\bar{q}_{ecf}$ from the following:

$$\begin{aligned}
& {}^{ecf}\bar{q}_{m,i}^{-1} \otimes {}^{ecf}\bar{q}_{m,j} \\
&= {}^{gim}\bar{q}_{ecf}^{-1} \otimes {}^{tel}\bar{q}_{gim,-ij} \otimes {}^{gim}\bar{q}_{ecf} \quad (8) \\
&= \begin{bmatrix} A\left({}^{gim}\bar{q}_{ecf}^{-1}\right) & 0 \\ 0 & 1 \end{bmatrix} {}^{tel}\bar{q}_{gim,-ij}
\end{aligned}$$

where

$${}^{tel}\bar{q}_{gim,-ij} = {}^{tel}\bar{q}_{gim,i}^{-1} \otimes {}^{tel}\bar{q}_{gim,j} \quad (9)$$

Note that the alignment is calculated by ignoring the measurement noise, so the solution is not expected to be optimal. However, the result from this coarse alignment calculation is sufficient to use as the initial value for the fine calibration described in the next section.

Fine Alignment Calibration

The fine alignment calibration is done by nonlinear least squares. By minimizing the error between the star camera quaternion measurements and the expected measurements calculated from the estimated states, the best alignment estimate can be determined. We use two notations to represent error quaternion and the current estimate of quaternion as $\delta\bar{q}$ and \hat{q} respectively, so that $\bar{q} = \delta\bar{q} \otimes \hat{q}$. Using this notation, (2) becomes

$$\begin{aligned}
\bar{q}_{m,i} &= \bar{q}_{n,i} \otimes \delta^{cam}\bar{q}_{tel} \otimes {}^{cam}\hat{q}_{tel} \otimes {}^{tel}\bar{q}_{gim,i} \\
&\otimes \delta^{gim}\bar{q}_{ecf} \otimes {}^{gim}\hat{q}_{ecf} \otimes {}^{ecf}\bar{q}_{j2k,i} \quad (10)
\end{aligned}$$

and the current estimated star camera quaternion measurement is

$$\hat{q}_{m,i} = {}^{cam}\hat{q}_{tel} \otimes {}^{tel}\bar{q}_{gim,i} \otimes {}^{gim}\hat{q}_{ecf} \otimes {}^{ecf}\bar{q}_{j2k,i} \quad (11)$$

We can calculate the error quaternion between (10) and (11) as

$$\begin{aligned}
\delta\bar{q}_{m,i} &= \bar{q}_{m,i} \otimes \hat{q}_{m,i}^{-1} \\
&= \bar{q}_{n,i} \otimes \delta^{cam}\bar{q}_{tel} \otimes {}^{cam}\hat{q}_{tel} \otimes {}^{tel}\bar{q}_{gim,i} \\
&\otimes \delta^{gim}\bar{q}_{ecf} \otimes \left({}^{cam}\hat{q}_{tel} \otimes {}^{tel}\bar{q}_{gim,i} \right)^{-1} \\
&= \bar{q}_{n,i} \otimes \delta^{cam}\bar{q}_{tel} \otimes \begin{bmatrix} A\left({}^{cam}\hat{q}_{gim,i}\right) & 0 \\ 0 & 1 \end{bmatrix} \delta^{gim}\bar{q}_{ecf} \quad (12)
\end{aligned}$$

where

$${}^{cam}\hat{q}_{gim,i} = {}^{cam}\hat{q}_{tel} \otimes {}^{tel}\bar{q}_{gim,i} \quad (13)$$

If we take the vector part of (12), the error quaternion vector can be approximated as

$$\delta\vec{q}_{m,i} = \vec{q}_{n,i} + \delta^{cam}\vec{q}_{tel} + A\left({}^{cam}\hat{q}_{gim,i}\right)\delta^{gim}\vec{q}_{ecf} \quad (14)$$

With several measurements, we can formulate the measurement equation as

$$\begin{bmatrix} \delta\vec{q}_{m,1} \\ \vdots \\ \delta\vec{q}_{m,n} \end{bmatrix} = \begin{bmatrix} I & A\left({}^{cam}\hat{q}_{gim,1}\right) \\ \vdots & \vdots \\ I & A\left({}^{cam}\hat{q}_{gim,n}\right) \end{bmatrix} \begin{bmatrix} \delta^{cam}\vec{q}_{tel} \\ \delta^{gim}\vec{q}_{ecf} \end{bmatrix} + \begin{bmatrix} \vec{q}_{n,1} \\ \vdots \\ \vec{q}_{n,n} \end{bmatrix} \quad (15)$$

This is the form of

$$\delta\vec{y}_k = H\delta\vec{x}_k + \vec{v} \quad (16)$$

where k is the iteration number. Using least squares,

$$\delta\vec{x}_k = \left(H^T R^{-1} H \right)^{-1} H^T R^{-1} \delta\vec{y}_k = \begin{bmatrix} \delta^{cam}\vec{q}_{tel} \Big|_k \\ \delta^{gim}\vec{q}_{ecf} \Big|_k \end{bmatrix} \quad (17)$$

where

$$R = \text{diag}(r_1, r_2, r_3, r_1, r_2, r_3, \dots, r_3) \quad (18)$$

Then, the alignment quaternions can be updated for the next iteration as

$$\begin{aligned}
{}^{cam}\hat{q}_{tel} \Big|_{k+1} &= \begin{bmatrix} \delta^{cam}\vec{q}_{tel} \Big|_k \\ 1 \end{bmatrix} \otimes {}^{cam}\hat{q}_{tel} \Big|_k \\
{}^{gim}\hat{q}_{ecf} \Big|_{k+1} &= \begin{bmatrix} \delta^{gim}\vec{q}_{ecf} \Big|_k \\ 1 \end{bmatrix} \otimes {}^{gim}\hat{q}_{ecf} \Big|_k \quad (19)
\end{aligned}$$

The fine alignment calibration uses the result of the coarse alignment calculation, the solution of (6) and (8), as the initial values of the alignment, ${}^{cam}\hat{q}_{tel} \Big|_0$ and ${}^{gim}\hat{q}_{ecf} \Big|_0$.

ALGORITHMS FOR TRACKING

To track a satellite, we need to calculate the gimbal angles, Azi and Alt, and the rate of each. In this section we derive the analytical solution for Azi and Alt angles as well as their rates for a given position and velocity of a satellite, which is estimated from the SGP4.

Gimbal Angle Command

Let \vec{l}_{cam} be the unit LOS vector of the telescope in the camera frame, which is obtained by manual calibration as described in the previous section, and let \vec{r}_{j2k} be the unit pointing vector from the telescope to a satellite in the ECI frame, calculated as

$$\vec{r}_{j2k} = \frac{\vec{R}_{sat,j2k} - \vec{R}_{GS,j2k}}{|\vec{R}_{sat,j2k} - \vec{R}_{GS,j2k}|} \quad (20)$$

where $\vec{R}_{sat,j2k}$ is the position of a satellite and $\vec{R}_{GS,j2k}$ is the position of the GS in J2000 frame. In order to point the telescope LOS towards the satellite, the following equation should be satisfied.

$$\vec{l}_{cam} = {}^{cam}T_{tel} {}^{tel}T_{gim} {}^{gim}T_{ecf} {}^{ecf}T_{j2k} \vec{r}_{j2k} \quad (21)$$

where bT_a represent a DCM from a frame to b frame. ${}^{cam}T_{tel}$ and ${}^{gim}T_{ecf}$ are estimated from the alignment calibration that is described in the previous section, ${}^{ecf}T_{j2k}$ is calculated from the IERS Earth model, and ${}^{tel}T_{gim}$ is given as (1). Reorganizing (21),

$$\vec{l}_{tel} = {}^{tel}T_{gim} \vec{r}_{gim} \quad (22)$$

where

$$\vec{l}_{tel} = {}^{tel}T_{cam} \vec{l}_{cam} \quad (23)$$

$$\vec{r}_{gim} = {}^{gim}T_{ecf} {}^{ecf}T_{j2k} \vec{r}_{j2k} \quad (24)$$

From (1) and (22),

$$\begin{bmatrix} l_1 \\ l_2 \\ l_3 \end{bmatrix} = \begin{bmatrix} cz & 0 & -sz \\ st \cdot sz & ct & st \cdot cz \\ ct \cdot sz & -st & ct \cdot cz \end{bmatrix} \begin{bmatrix} r_1 \\ r_2 \\ r_3 \end{bmatrix} \quad (25)$$

where $\vec{l}_{gim} = [l_1 \ l_2 \ l_3]^T$ and $\vec{r}_{gim} = [r_1 \ r_2 \ r_3]^T$. By expanding (25), we obtain three equations as

$$l_1 = r_1 \cos z - r_3 \sin z \quad (26)$$

$$l_2 = r_1 \sin t \sin z + r_2 \cos t + r_3 \sin t \cos z \quad (27)$$

$$l_3 = r_1 \cos t \sin z - r_2 \sin t + r_3 \cos t \sin z \quad (28)$$

From (26), the Azi angle can be solved analytically and the Alt angle can be solved from (27) and (28).

Gimbal Angle Rate Command

To calculate the Azi and Alt rates, let us consider the time derivative of the LOS vector in the telescope frame (22) as

$$\dot{\vec{l}}_{tel} = {}^{tel}\dot{T}_{gim} \vec{r}_{gim} + {}^{tel}T_{gim} \dot{\vec{r}}_{gim} \quad (29)$$

Since the telescope LOS is fixed in the telescope frame, $\dot{\vec{l}}_{tel} = 0$. Then, the time derivative of the LOS in the gimbal frame is given as

$$\dot{\vec{r}}_{gim} = -{}^{tel}T_{gim}^{-1} {}^{tel}\dot{T}_{gim} \vec{r}_{gim} \quad (30)$$

By taking the derivative of (1),

$${}^{tel}\dot{T}_{gim} = \dot{T}Z + T\dot{Z} \quad (31)$$

where

$$T = \begin{bmatrix} 1 & 0 & 0 \\ 0 & ct & st \\ 0 & -st & ct \end{bmatrix}, \quad Z = \begin{bmatrix} cz & 0 & -sz \\ 0 & 1 & 0 \\ sz & 0 & cz \end{bmatrix} \quad (32)$$

and

$$\dot{T} = \dot{t} \begin{bmatrix} 0 & 0 & 0 \\ 0 & -st & ct \\ 0 & -ct & -st \end{bmatrix}, \quad \dot{Z} = \dot{z} \begin{bmatrix} -sz & 0 & -cz \\ 0 & 0 & 0 \\ cz & 0 & -sz \end{bmatrix} \quad (33)$$

From (30)-(33),

$$\begin{aligned} {}^{tel}T_{gim}^{-1} {}^{tel}\dot{T}_{gim} &= Z^{-1}T^{-1}\dot{T}Z + Z^{-1}T^{-1}T\dot{Z} \\ &= \begin{bmatrix} 0 & -\dot{t} \sin z & -\dot{z} \\ \dot{t} \sin z & 0 & \dot{t} \cos z \\ \dot{z} & -\dot{t} \cos z & 0 \end{bmatrix} \end{aligned} \quad (34)$$

$$\begin{bmatrix} \dot{r}_1 \\ \dot{r}_2 \\ \dot{r}_3 \end{bmatrix} = \begin{bmatrix} \dot{t} r_2 \sin z + \dot{z} r_3 \\ -\dot{t} r_1 \sin z - \dot{t} r_3 \cos z \\ \dot{t} r_2 \cos z - \dot{z} r_1 \end{bmatrix} \quad (35)$$

From (35), the Azi and Alt rate corresponding to the desired $\dot{\vec{r}}_{gim}$ can be calculated as

$$\dot{z} = \frac{\dot{r}_1 \cos z - \dot{r}_3 \sin z}{r_1 \sin z + r_3 \cos z} \quad (36)$$

$$\dot{i} = -\frac{\dot{t}_2}{r_1 \sin z + r_3 \cos z} \quad (37)$$

Gimbal Control Law

The CPC 1100 telescope is a COTS amateur telescope that can be controlled with Azi and Alt slew rates as input commands. The telescope also takes Azi/Alt or RA/DEC angle commands, but the Azi/Alt angle command has very large overshoot and the RA/DEC command can only be used after the built-in alignment calibration. Since the dynamics of the gimbal mount are unknown and we also have no information about the internal control loop, we set up a simple control law that command Azi Alt rate as

$$\begin{aligned} \dot{z}_c &= \dot{z}_d + \frac{1}{T_s}(z_d - z_r) \\ \dot{t}_c &= \dot{t}_d + \frac{1}{T_s}(t_d - t_r) \end{aligned} \quad (38)$$

where \dot{z}_d and \dot{t}_d are the desired Azi and Alt slew rates that are calculated from (36) and (37), and z_d and t_d are the desired Azi and Alt angles calculated from (26)-(28) respectively. z_r and t_r are the current Azi and Alt angle reading from the telescope mount. T_s is the settling time for the error angle compensation, the value of which was selected by trial-and-error as 0.3 sec. This test was conducted in an indoor lab since we only need to compare the measured mount angles to the commanded mount angles. We generated a mount angle and slew rate profile for a sample International Space Station (ISS) tracking case whose maximum elevation angle is 35 deg. This case is used to check that the control law given by (38) works properly. With T_s of 0.3 sec, we obtain the following tracking results:

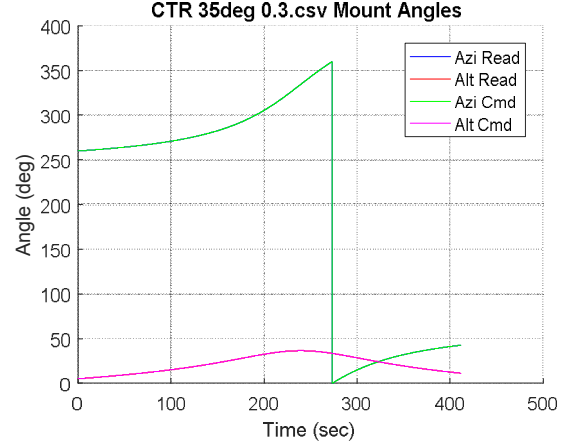


Figure 4: Azi/Alt mount angles measured for a sample ISS tracking maneuver.

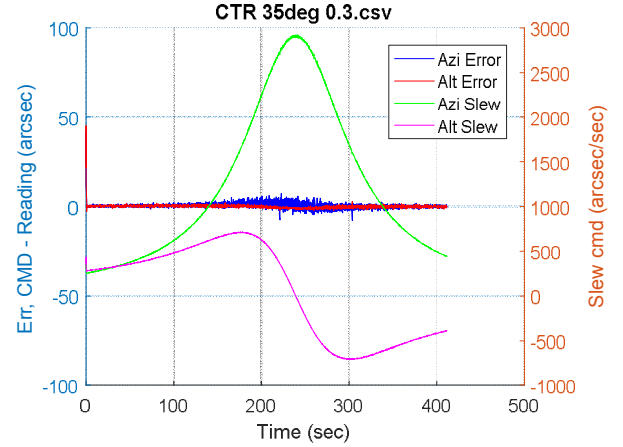


Figure 5: Azi/Alt control error plotted with the slew rate commands.

Figure 4 shows the Azi/Alt angle profiles measured from the mount for the ISS tracking maneuver. Figure 5 shows the angle errors, $z_d - z_r$ and $t_d - t_r$, as well as the commanded slew rates. This plot shows that the system experiences lagging when the slew rate is high (> 1000 arcsec/sec), but the error is within 10 arcsec which is sufficient to capture the ISS considering the FOV of 282 arcsec x 212 arcsec in this scenario.

Closed-loop Feedback Control

If there is no error or noise in the telescope tracking, we do not need feedback control. However, there are several error sources that can occur in actual satellite tracking, so we need to feed back the satellite's position measured by some sensing device to counteract drift.

In the optical ground station configuration, an IR camera is used to measure the relative pointing vector to the satellite. However, for ease of testing, we verified our approach by tracking the ISS in the visible wavelengths by using the star camera. The purpose of the star camera is initial alignment calibration, so it is not performing any functions during the tracking. In lieu of an IR camera, we can test the approach using the star camera for visible feedback.

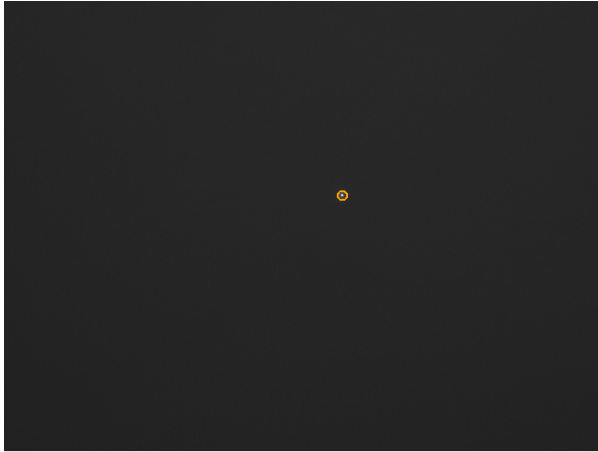


Figure 6: The ISS (orange circle) as seen in the star camera.

Figure 6 is the ISS image taken by the star camera. If there is no obstruction, the ISS is the only bright object on the image since the stars are blurred by the tracking motion of the telescope. This makes it easy to identify the ISS and feed back its position on the image.

TEST RESULTS

To verify our approach, we conducted several tracking experiments of the ISS. This section presents a sample ISS tracking result. The test was done on 05/26/2016 at 07:14:00 to 07:21:31 UTC on the rooftop of an MIT building.

Alignment Calibration Results

The first step of the ISS tracking is the alignment calibration. The GS software automatically plans the star imaging schedule with different gimbal angles and executes the alignment process. It rotates the telescope to 18 different gimbal angles and captures images with the star camera. Once it has finished its scan, the alignment is calculated by the method previously described. After the calibration, two residual errors are used as accuracy metrics to evaluate performance.

The first metric is the residual error of the star vectors in each star image. This provides an estimate of the accuracy for each individual star camera image. Once an attitude quaternion is calculated from the star vectors for a star pattern image, we can calculate the expected position of the stars on the image. Then, the difference between the measured star vectors and the expected star vectors is calculated.

The second metric is the residual of the attitude quaternions from the star images. This provides an estimate of the global calibration accuracy. When the alignment calibration is finished, the residual of the error quaternion, defined as

$$\delta \bar{q}_{m,i} = \bar{q}_{m,i} \otimes \hat{q}_{m,i}^{-1} \quad (39)$$

where $\hat{q}_{m,i}$ is given by (11), is calculated. Table 1 shows the alignment results. In this ISS tracking test, 12 out of 18 star pattern images are used for the calibration. The 6 images rejected for calibration do not have enough observed stars due to clouds or other visual obstructions.

The root-mean-square (RMS) error of the star vectors are 10-20 arcsec within each image, which means the expected attitude accuracy for each measurement is 10-20 arcsec (1σ) in the cross-boresight direction, or X and Y axes of the star camera frame. However, the residual quaternion errors in the cross-boresight direction go up to 220 arcsec, which is substantially more than the star vector residual RMS of 10-20 arcsec. The residual errors in the star camera frame are the very close to the expected pointing errors in the telescope frame since the LOS of the telescope is very close to the Z axis of camera frame. Since the FOV of the telescope with the eyepiece camera is 282 arcsec x 212 arcsec, if the pointing error is more than 106 arcsec, the ISS will not be captured on the eyepiece camera.

There are several sources of the large errors seen in the global accuracy residuals. We hypothesize that a major source of error is due to the deformation of the mount as well as the deformation of the non-rigid floor. The telescope and the gimbal mount are on a tripod, which lacks the structural stability of standard ground stations. Additionally, no housing is used for this test and wind can significantly perturb the telescope. If the load on each leg of the tripod changes, the mount and floor will be deformed differently so that ${}^{sim}\bar{q}_{ecf}$ will not remain constant. For different Azi/Alt angles, the center of gravity will change, causing potentially significant error.

Another expected error source is timing error. The GS uses a Windows operating system rather than a real-time operating system (RTOS). The time is synchronized via the internet, so there can be errors up to 1 sec resulting in an incorrect value for ${}^{eef}\bar{q}_{j2k}$.

However, this is not the dominant error source since the Earth's rotation rate is small at 15 arcsec/sec, whereas the residual quaternion error goes up to 200 arcsec.

Table 1: Results from alignment calibration.

No.	# of Stars	Azi (deg)	Alt (deg)	RMS residual star vector (arcsec)	Residual quaternion, X-axis (arcsec)	Residual quaternion, Y-axis (arcsec)	Residual quaternion, Z-axis (arcsec)
1	12	360.00	30.00	10.01	197.29	-10.45	-106.61
2	9	60.00	30.00	18.93	-100.51	-147.90	-206.55
3	11	180.00	30.00	22.75	-49.46	133.01	-9.29
4	12	288.00	43.75	12.63	73.83	68.71	279.88
5	10	216.00	43.75	17.53	44.35	188.85	273.32
6	10	144.00	43.75	13.81	28.22	-24.09	-7.73
7	9	72.00	43.75	11.16	19.18	-176.87	-204.96
8	10	360.00	43.75	14.95	198.05	-2.35	-70.39
9	7	360.00	57.50	10.55	221.94	29.81	-32.71
10	10	90.00	57.50	16.27	0.91	-125.61	-206.30
11	6	180.00	57.50	20.08	45.55	47.51	100.33
12	9	180.00	71.25	20.51	72.91	11.93	191.01
RMS	n/a	n/a	n/a	16.28	113.99	104.48	169.4

Regardless of the source, certain pointing error does exist that goes up to 200 arcsec, which is much more than the half of the FOV of 106 arcsec. This means that open-loop control will not ensure that the ISS is captured by the telescope, so we need feedback control of the ISS pointing vector to enable tracking.

ISS Tracking Results

With the alignment calibrated, we can track the ISS. Unlike in the case of alignment calibration, the timing error during tracking cause large errors since the satellite is moving at >7 km/sec. This error can be compensated by closed-loop feedback control.

As mentioned previously, the star camera was used as the tracking sensor of the ISS. The ISS vector update period was 3 to 4 sec. According to the iNova camera manual, it can achieve 30 frames per second (fps), but it was not possible with the iNova SDK 1.2.4 in C#. The feedback frequency of ~0.3 Hz was not high, but it is sufficient to capture the ISS in the 282 arcsec x 212 arcsec FOV.

During the test, we recorded a video of the ISS and Figure 7 shows a screen capture of the video. The ISS

stays in the screen most of time when it uses the feedback control, although it is floating around on the screen. The floating motion is expected to be due to the low feedback frequency, but the IR camera to be integrated in the next steps will have a much higher feedback rate.

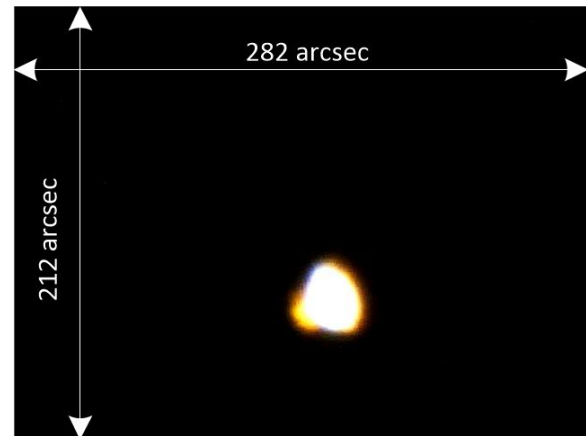


Figure 7: The ISS captured on the eyepiece camera.

Figure 8 and Figure 9 shows the Azi/Alt angle profiles and the control errors similar to Figure 4 and Figure 5. The control error, shown in Figure 9, is defined as the difference between the commanded angles and the angles measured from the telescope mount. It is not a measure of true error, but rather how well the mount is tracking input commands. The first feedback was applied at 117 sec after the tracking start, which appears as the first huge peak on Figure 9. The magnitude of the angle error at the first feedback was 828 arcsec which is the initial open-loop pointing error. The first feedback time was 117 sec after the tracking start due to visual obstructions in the FOV of the star camera.

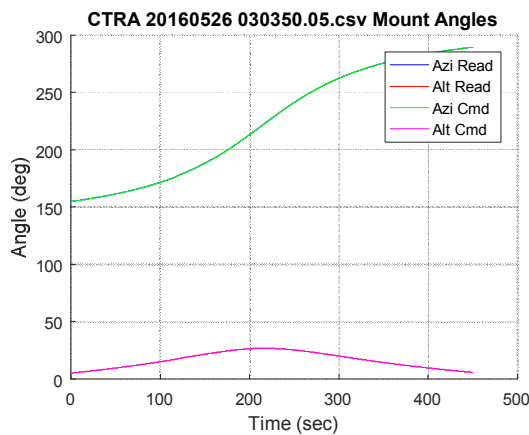


Figure 8: Azi/Alt angle profile for the ISS tracking

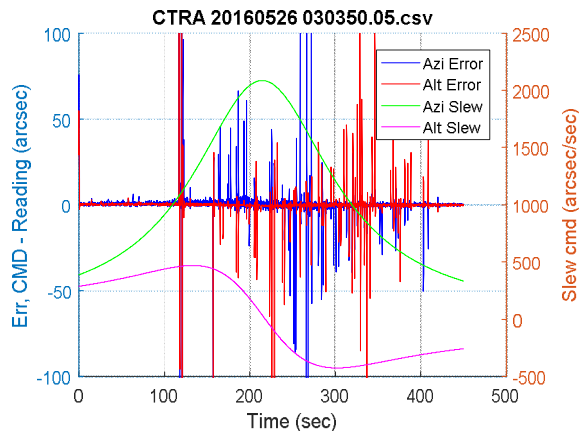


Figure 9: Azi/Alt control error and slew rate command.

Figure 10 shows the ISS tracking error during the tracking. The error is the off-center distance of ISS image center and is calculated from each frame of the video. The RMS error through the tracking is 42.814 arcsec in X axis and 36.337 arcsec in Y axis, or 56.15 arcsec in total.

From this test result, we can conclude that it is possible to track a satellite with an amateur telescope. There are several improvements that can be made to the setup and also some fundamental limitations. The telescope is limited to lower elevations due to the keyhole problem. At high elevations, the slew rates required of the Azi/Alt gimbals can exceed 3.5 deg/s, which is the limitation imposed by the motors. In this situation, without further modification of the actual motor controller in the telescope, the telescope will fail to track near peak, but it can pick up the satellite again on the trailing side. Improvements and further work are discussed in the concluding section.

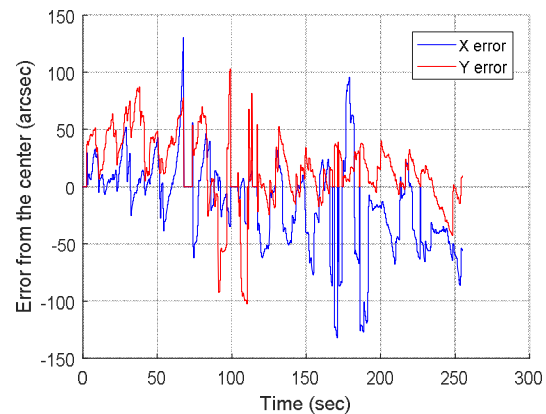


Figure 10: The ISS tracking error, calculated from location on the eyepiece camera.

CONCLUSION

In this study, we developed a satellite tracking system using an amateur telescope. All equipment used in this study comes from commercial off-the-shelf (COTS) parts and the tracking software was developed by the authors. An alignment calibration method using a star camera was proposed and tested in hardware. The tracking algorithms were derived and also tested by tracking the International Space Station (ISS). The experiment result shows that it is possible to track the ISS within the eyepiece camera's field-of-view (FOV) of 282 arcsec x 212 arcsec. The root-mean-square error of the ISS tracking was 56.12 arcsec, the remainder of which can be corrected by the fine pointing system.

FUTURE WORK

The next steps are aimed at improving tracking accuracy and transitioning to the use of the IR camera for closed-loop tracking. The feedback approach described in the ISS tracking results section was a partially manual process. While the software autonomously identified the brightest object in the frame, the command to center on that object was

executed manually. This was a conservative approach to the initial testing that allowed external verification that the ISS was correctly identified. The next step is to modify the software to use autonomous, closed loop feedback to identify the ISS. Criteria for identifying the ISS and robustness against obstructions or fades must be implemented in software.

This approach will first be implemented and tested using the star camera for closed loop feedback. Once the approach is validated with the star camera, the next step will be to transition to the IR camera. This will require development of the mounting apparatus to the telescope that incorporates the FSM and IR camera instead of the eyepiece camera. The final piece of ground station pointing is to implement the fine pointing loop with the FSM, which will rely on the software developed for satellite identification and tracking.

ACKNOWLEDGMENTS

We acknowledge the support of the MIT Deshpande Center and its Innovation Grant that has provided funding for this work. Hyosang Yoon acknowledges the financial support from Samsung Scholarship.

REFERENCES

1. Boroson, D. M., Robinson, B. S., Murphy, D. V., Burianek, D. A., Khatri, F., Kovalik, J. M., Sodnik, Z., and D.M. Cornwell, "Overview and results of the Lunar Laser Communication Demonstration," SPIE Photonics West 2014-LASE: Lasers and Sources, vol. 8971, 2014.
2. Witting et al., M., "Status of the European Data Relay Satellite System," Proceedings of the International Conference on Space Optical Systems and Applications, 2012.
3. Kingsbury, R., Riesing, K., and K. Cahoy, "Design of a Free-Space Optical Communication Module for Small Satellites," 28th Annual AIAA/USU Conference on Small Satellites, 2014.
4. Gouy, Y., Wang, Q., d'Humières, B., Sanchez, C. Q., O'Brien, D., Platt, D., Krezel, J., Salter, M., Michalkiewicz, A., Wagner, P., Steck, E., Theux, Y., Vourch, S., and W. Riede, "Advanced concept for laser communication system for micro and nanosatellites," Proc. of Small Satellites, System & Services Symposium, 2016.
5. Janson, S. W., and R. P. Welle, "The NASA Optical Communication and Sensor Demonstration Program: An Update," Proceedings of the 28th Annual AIAA/USU Conference on Small Satellites, 2014.
6. Biswas, A., Kovalik, J. M., Wright, M. W. and W. T. Roberts, "Optical Communications Telescope Laboratory (OCTL) Support of Space to Ground Link Demonstrations," Proceedings of SpaceOps Conference, 2014.
7. Berkefeld, T., Soltau, D., Czichy, R., Fischer, E., Wandernoth, B., and Z. Sodnik, "Adaptive optics for satellite-to-ground laser communication at the 1m Telescope of the ESA Optical Ground Station, Tenerife, Spain," Proc. SPIE 7736, Adaptive Optics Systems II, 2010.
8. Shrestha, A. and M. Brechtelsbauer, "Transportable optical ground station for high-speed free-space laser communication," Proc. SPIE 8517, Laser Communication and Propagation through the Atmosphere and Oceans, 2012.
9. Moll, F., Mitzkus, W., Horwath, J., Shrestha, A., Brechtelsbauer, M., Navajas, L. M., Souto, A. L., Gonzalez, D. D., "Demonstration of high-rate laser communications from fast airborne platform: flight campaign and results", Proc. SPIE 9248, p. 92480R, 2014.
10. Vallado, D. A., and Crawford, P., "SGP4 orbit determination." Proceedings of AIAA/AAS Astrodynamics Specialist Conference and Exhibit. 2008.
11. Petit, G., and Brian, L., "IERS Conventions (2010)," IERS Technical Note No. 36, 2010, ISBN 3-89888-989-6.
12. Yoon, H., Lim, Y., and Bang, H., "New Star-Pattern Identification Using a Correlation Approach for Spacecraft Attitude Determination," *Journal of Spacecraft and Rockets*, 48, 1, 182-186, 2011.
13. Yoon, H., Paek, S. W., Lin, Y., Lee, B. H., and Lee, H., "New star pattern identification with vector pattern matching for attitude determination," *IEEE Transactions on Aerospace and Electronic Systems*, 49, 2, 1108-1118, 2013.
14. Shuster, M. D., and Oh, S. D., "Three-axis attitude determination from vector observations," *AIAA Journal of Guidance, Control, and Dynamics*, 4, 1, 70-77, 1981.